Advanced Composite Materials
Publication details, including instructions for authors and subscription information:
http://www.tandfonline.com/loi/tacm20

Tensile strength of unidirectional CFRP laminate under high strain rate

Norihiko Taniguchi [a], Tsuyoshi Nishiwaki [b] & Hiroyuki Kawada [c]
[a] R&D Department, ASICS Corporation 6-2-1 Takatsukadai, Nishi-ku, Kobe 651-2271, Japan
[b] R&D Department, ASICS Corporation 6-2-1 Takatsukadai, Nishi-ku, Kobe 651-2271, Japan
[c] Department of Mechanical Engineering, Waseda University, Tokyo, Japan
Version of record first published: 02 Apr 2012.

To cite this article: Norihiko Taniguchi , Tsuyoshi Nishiwaki & Hiroyuki Kawada (2007): Tensile strength of unidirectional CFRP laminate under high strain rate, Advanced Composite Materials, 16:2, 167-180

To link to this article: http://dx.doi.org/10.1163/156855107780918937

Adv. Composite Mater., Vol. 16, No. 2, pp. 167–180 (2007)

Also available online - www.brill.nl/acm

Tensile strength of unidirectional CFRP laminate under high strain rate

NORIHIKO TANIGUCHI [1,*], TSUYOSHI NISHIWAKI [1] and HIROYUKI KAWADA [2]

[1] *R&D Department, ASICS Corporation 6-2-1 Takatsukadai, Nishi-ku, Kobe 651-2271, Japan*
[2] *Department of Mechanical Engineering, Waseda University, Tokyo, Japan*

Received 20 April 2006; accepted 31 July 2006

Abstract—The tensile strength of unidirectional carbon fiber reinforced plastics under a high strain rate was experimentally investigated. A high-strain-rate test was performed using the tension-type split Hopkinson bar technique. In order to obtain the tensile stress–strain relations, a special fixture was used for the impact tensile specimen. The experimental results demonstrated that the tensile modulus and strength in the longitudinal direction are independent of the strain rate. In contrast, the tensile properties in the transverse direction and the shear properties increase with the strain rate. Moreover, it was observed that the strain-rate dependence of the shear strength is much stronger than that of the transverse strength. The tensile strength of off-axis specimens was measured using an oblique tab, and the experimental results were compared with the tensile strength predicted based on the Tsai–Hill failure criterion. It was concluded that the tensile strength can be characterized quite well using the above failure criterion under dynamic loading conditions.

Keywords: CFRP; split Hopkinson bar; strain-rate effect; tensile strength; failure criterion; off-axis test.

1. INTRODUCTION

Carbon fiber reinforced plastic (CFRP) laminates have been recognized for their high performance and good mechanical properties. Therefore, they have been widely used not only in the aerospace industry but also to manufacture sports gear. In order to create practical designs of CFRP laminates for a variety of sports gear, it is essential that they possess excellent mechanical properties under a dynamic load [1, 2]. Nevertheless, it is quite difficult to experimentally determine these properties, such as the modulus and strength.

Edited by the JSCM.

*To whom correspondence should be addressed. E-mail: nori@tiger4.sp.asics.co.jp

Several studies have attempted to evaluate the above properties. Staab and Gilat [3] investigated the effects of tensile strength in the case of angle-ply glass/epoxy laminates. They concluded that the fibers had a greater influence on the strain-rate effect than the matrix. The strain-rate dependence of the interlaminar shear strength was deduced by Harding and Li [4]. In that study, a double-lap shear specimen was used as the basis of the finite element method. The interlaminar shear strength was found to increase significantly with the strain rate. Tsai and Sun [5] investigated and proposed a mechanical model for the dynamic compressive behavior of glass/epoxy composites. A viscoplasticity model was incorporated with Rosen's fiber buckling model [6] to predict the compressive strength at a high strain rate. Harding and Welsh [7] developed a technique for the impact tensile testing of a unidirectional composite by modifying the split Hopkinson bar (SHB) method. It has been shown that the tensile strength and failure mode of CFRPs are independent of the strain rate. However, the failure criterion at a high strain rate has not yet been examined.

Recently, Thiruppukuzhi and Sun [8] characterized the strain-rate-dependent behavior of two different polymeric composite materials. In that study, a three-parameter viscoplasticity model was developed for predicting the nonlinear strain-rate-dependent behavior. Although the model prediction was in good agreement with the experimental data, the maximum strain rate, i.e. 1.0 s^{-1}, was not sufficient since the experimental technique for determining the tensile strength at a high strain rate is a difficult task.

In this study, the tensile strength of a unidirectional CFRP under a high strain rate is measured by using a tension-type SHB apparatus [9, 10]. A special fixture is used for the impact tensile specimen. By using this fixture technique, the strain-rate dependence of the tensile properties (in the longitudinal and transverse directions) and the shear properties are investigated. The dynamic tensile strength of off-axis specimens is evaluated using an oblique tab. Finally, the failure criterion is discussed for predicting the tensile strength at a high strain rate.

2. EXPERIMENTAL

2.1. Specimens

The specimens were fabricated by stacking T700S/2500 composite prepregs (Toray Industries, Inc., volume fraction of fiber, $v_f = 67\%$) by using the vacuum-bag method. The end tabs were cut from $\pm 45^\circ$ carbon/epoxy panels and then bonded onto the specimens. In order to obtain the tensile properties for each material principal direction under a high strain rate, three values of the fiber orientation angle θ are employed. In other words, the tensile properties in the longitudinal and transverse directions are evaluated with the $\theta = 0^\circ$ and $\theta = 90^\circ$ specimens, respectively. The shear properties are evaluated with the $\theta = [\pm 45]_s$ specimen [11]. The geometry of the specimen is shown in Fig. 1, and its specifications are presented in Table 1.

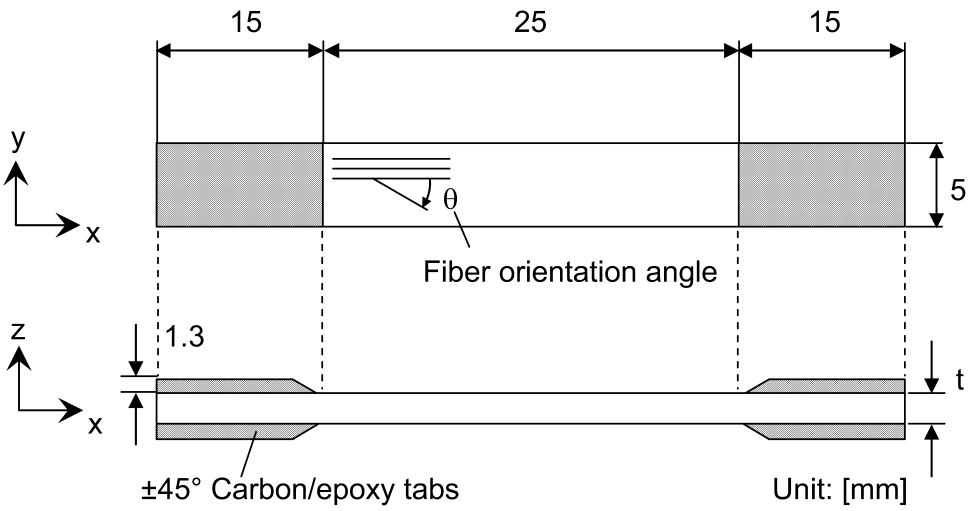

Figure 1. Geometry of the specimen.

Table 1.
Specifications of the specimen for each material direction

Material principal direction	Longitudinal	Transverse	Shear
Stacking sequence	0	90	$[\pm 45]_s$
Thickness [mm]	0.125 (1 ply)	2.0	2.0

2.2. Experimental method

The tension-type SHB system is employed in this study. It consists of an input bar (length: 2000 mm, diameter: 16 mm, steel) with a flange, an output bar (length: 1500 mm, diameter: 16 mm, steel), and a cylindrical striker (length: 500 mm, outer and inner diameters: 22.8 mm and 16.2 mm, steel), as shown in Fig. 2(a). In order to control the fluctuating behavior during tensile loading, a piece of brass (outer and inner diameters: 22.0 mm and 16.2 mm, thickness: 1.0–5.0 mm) is sandwiched between the cylindrical striker and input bar [2]. The data obtained from the SHB method comprise the strain histories of the input and output bars. In the present study, the strain histories are recorded from strain gauges with a gauge length of 1.0 mm at a sampling rate of 1.0 MHz via a DC amplifier (upper frequency limit: 100 kHz). A general-purpose foil (KFG-1-350-C1-11, Kyowa Electronic Instruments Co., Ltd.) and semiconductor strain gauges (KSP-1-350-E4, Kyowa Electronic Instruments Co., Ltd.) are glued on the input and output bars, respectively.

An important issue in the construction of the tension-type SHB is the fixing of the specimen without causing it to slip. Ross *et al.* [9] proposed a dumbbell-type specimen with a special specimen holder. However, the disadvantages of this method are that it takes time to machine the specimen and it is difficult to use a plate-like specimen. Staab and Gilat [3] employed cement to fix the specimen

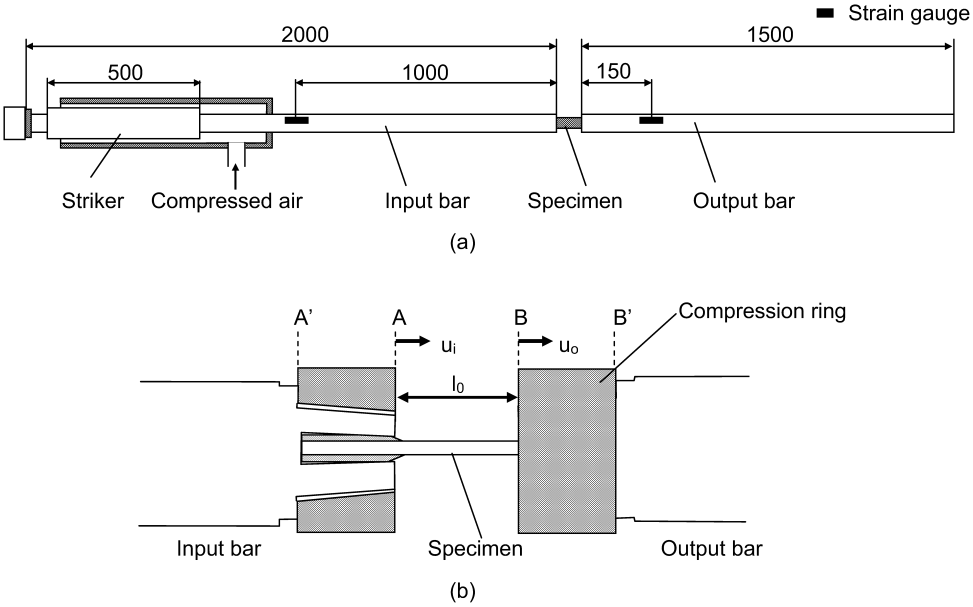

Figure 2. (a) Tension-type SHB apparatus. (b) A schematic drawing of the grip design.

between the input and output bars. Although this method provides a strong grip, it is very inconvenient. In this study, a special fixture for the impact tensile specimen is developed. The fixture design used in this study is illustrated in Fig. 2(b). The bar end has a tapered thread and a slot that is diametrically parallel to the region where the specimen is inserted. A saw-toothed slotted area is machined with precision. A compression ring with a thread, which compensates for the area loss caused by the slot, is mounted at the bar ends to fix the specimen. It was found that this fixing technique can transmit tensile loads of up to 2000 N.

3. EXPERIMENTAL RESULTS

3.1. Verification of the stress and strain in the specimens

Typical examples of the strain gauge outputs from the input and output bars for the 90° specimen are shown in Fig. 3(a). Due to the plastic deformation of the brass piece, it is observed that a ramped incident wave is produced. In the SHB system, the stress–strain relationship (σ–ε relationship) can be calculated by the one-dimensional wave propagation theory [12], that is,

$$\sigma = \frac{AE(\varepsilon_\mathrm{i} + \varepsilon_\mathrm{r})}{A_\mathrm{s}} = \frac{AE(\varepsilon_\mathrm{t})}{A_\mathrm{s}}, \tag{1}$$

$$\varepsilon = \frac{u_\mathrm{o} - u_\mathrm{i}}{l_0} = \frac{c_0}{l_0}\int_0^t (\varepsilon_\mathrm{t} - \varepsilon_\mathrm{i} - \varepsilon_\mathrm{r})\,\mathrm{d}\tau = -\frac{2c_0}{l_0}\int_0^t \varepsilon_\mathrm{r}\,\mathrm{d}\tau, \tag{2}$$

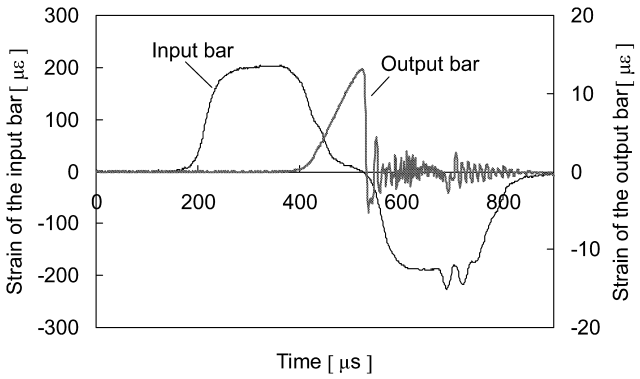

(a)

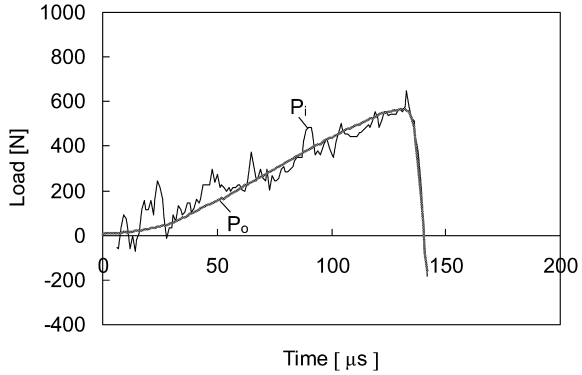

(b)

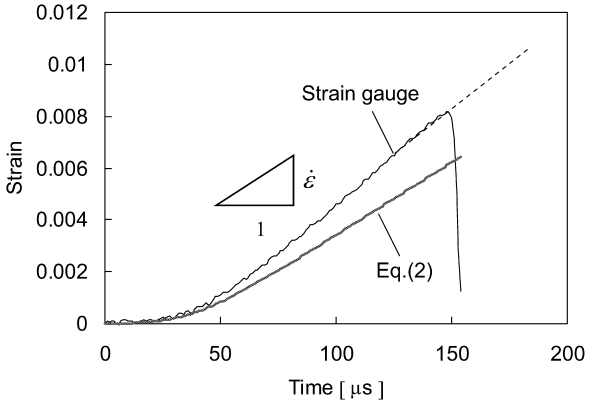

(c)

Figure 3. (a) Strain gauge outputs from the input and output bars for the 90° specimen. (b) Comparison of load histories at each face of the bars. (c) Comparison of strain histories between the strain gauge and conventional formulation.

where ε_i, ε_r, and ε_t denote the incident, reflected, and transmitted strain waves, respectively. Further, E denotes the bar's Young's modulus; A, the bar's cross-sectional area; c_0, the elastic wave speed; A_s, the specimen's cross-sectional area; and l_0, the specimen's gauge length. The parameters u_i and u_o denote the displacement of the specimen interface at the sides of the input and output bars, respectively. An important assumption that is made is that the wave propagation effects within the specimen are negligible. In other words, the load P_i between the input bar and specimen may be equivalent to the load P_o between the output bar and specimen (it follows that $\varepsilon_i + \varepsilon_r = \varepsilon_t$). Figure 3(b) shows a comparison of loads P_i and P_o for the 90° specimen. Although the time history of P_i seems to be very noisy, it agrees reasonably well with that of P_o. Therefore, the above assumption is applicable in this study. The tensile stress and strength can be determined from the transmitted strain wave. On the other hand, it is quite difficult to accurately calculate the strain. In order to verify the strain of the specimen, the strain histories calculated from equation (2) are compared with the output of the strain gauge glued on the specimen (Fig. 3(c)). It is clear that there is a large error in both the values. This result implies that the strain histories calculated from equation (2) are not applicable in this study. The strain of the specimen should be directly measured from the strain gauge glued on the specimen. Further, the strain rate $\dot{\varepsilon}$ can be calculated from the average slope of the strain histories as shown in Fig. 3(c).

3.2. Stress–strain curves

Typical examples of the stress–strain curves for the longitudinal, transverse, and shear directions, whose corresponding strain rates are approximately constant ($\dot{\varepsilon} = 100\ s^{-1}$), are shown in Fig. 4(a)–(c). The stress–strain curves for the static condition are also presented for comparison. A static test was carried out using a universal testing machine. The shear strain in Fig. 4(c) is calculated from the biaxial strain gauges. It is clear that the stress–strain curve for the longitudinal direction almost

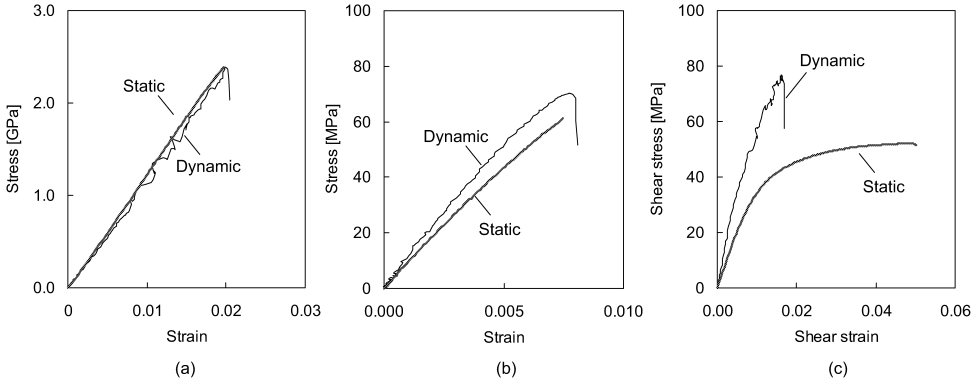

Figure 4. Typical examples of static and dynamic stress–strain curves: (a) Longitudinal direction; (b) Transverse direction; (c) Shear direction.

agrees with that for the static condition. This is the same tendency as that observed in the study by Harding and Welsh [7]. On the other hand, the dynamic stress–strain curves for the transverse and shear directions are quite different from that for the static condition. The modulus and strength are observed to increase. It should be noted that the failure position of the specimen is random but it is usually in the gauge section.

4. DISCUSSION

4.1. Dependence of the strain rate on mechanical properties

To investigate the dependence of the strain rate on mechanical properties, both the modulus and strength under various strain rates are measured. The relationships between the strain rate and the above properties are shown in Fig. 5(a) and (b). In the longitudinal direction, the strain rate has no effect on both the tensile modulus and strength, which are 125 ± 5.1 GPa and 2.33 ± 0.05 GPa, respectively. On the other hand, the mechanical properties in the transverse and shear directions are obviously affected by the strain rate. The tensile modulus and strength in the transverse direction increase linearly with the strain rate; they increase at the rates of 12.5% and 17.8% at 100 s^{-1}, respectively. Furthermore, the shear modulus and strength increase drastically with the strain rate; they increase at the rates of 77.1% and 77.5% at 100 s^{-1}, respectively. It is evident that these tendencies are primarily due to the viscoelasticity of the matrix [13]. The interesting point to note is that the shear strength exceeds the transverse strength at $\dot{\varepsilon} > 50$ s^{-1}. A fracture surface observation is carried out by using a scanning electron microscope (SEM). Figure 6(a) and (b) show the typical examples of a fracture surface under static and high-strain-rate conditions, respectively; the corresponding strain rates are 1.04×10^{-4} s^{-1} and 100 s^{-1}, respectively. In the fracture surface of the 90° specimen, it is clear that the crack propagates along the interface between the fiber and matrix. No significant difference can be observed between the static and high-strain-rate conditions. On the other hand, in the fracture surface of the $[\pm 45]_s$ specimen, it is observed that the configuration of the fracture surface changes drastically with the strain rate. The crack propagation area at $\dot{\varepsilon} = 100$ s^{-1} consists of not only the fiber/matrix interface but also the matrix itself, while that in the static condition is predominantly composed of the fiber/matrix interface. Based on these results, it is concluded that the shear strength of a unidirectional CFRP laminate is more sensitive than the transverse strength to the viscoelasticity of the matrix.

4.2. Dynamic tensile strength of the off-axis specimens

The 15°, 30°, 45°, 60° and 75° off-axis tensile specimens are tested under high-strain-rate conditions. One problem with the off-axis test is the extension-shear coupling effect [14]. To minimize this effect in the off-axis tensile test, a specimen

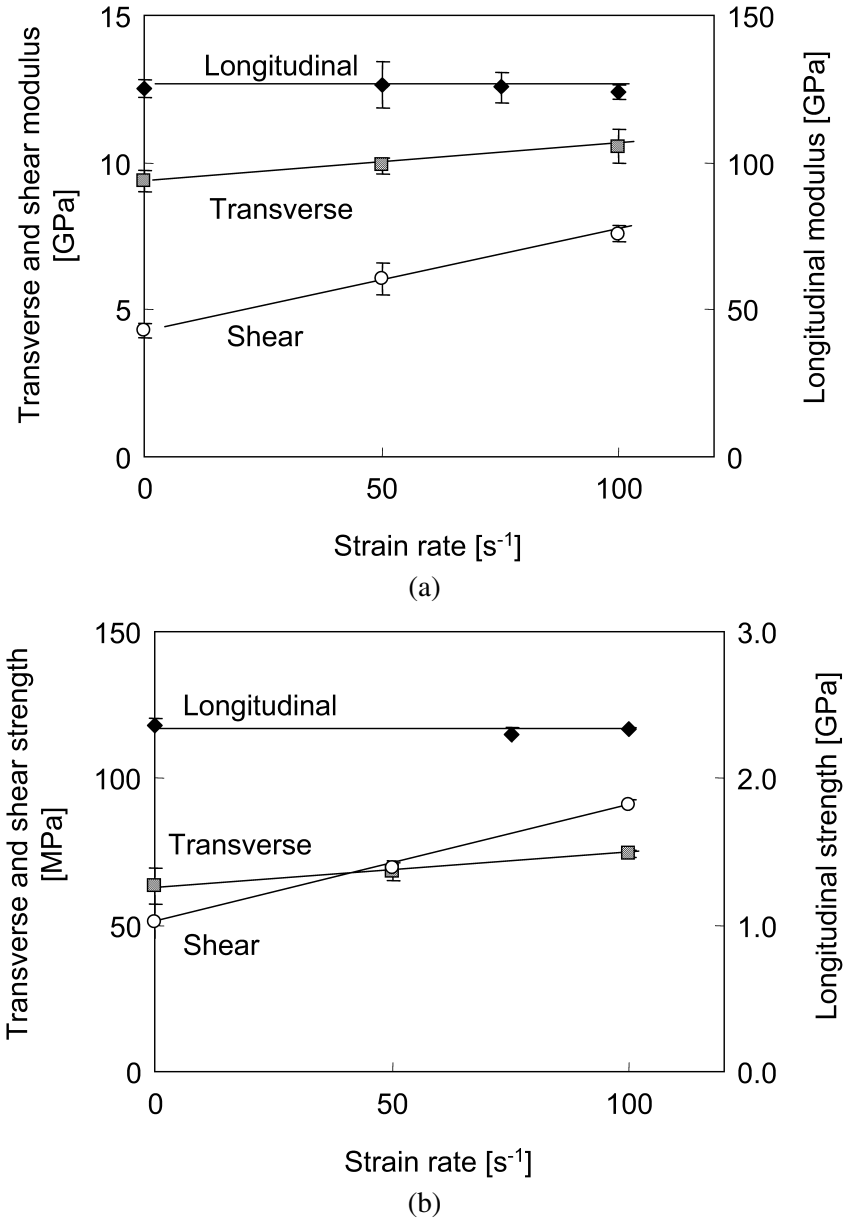

Figure 5. (a) Dependence of the strain rate on modulus. (b) Dependence of the strain rate on tensile strength.

with an aspect ratio that is in the range of 12–15 is recommended. However, it is practically difficult for a long specimen to achieve the high-strain-rate condition. In this study, an oblique end tab [15–17] is employed. According to a previous study,

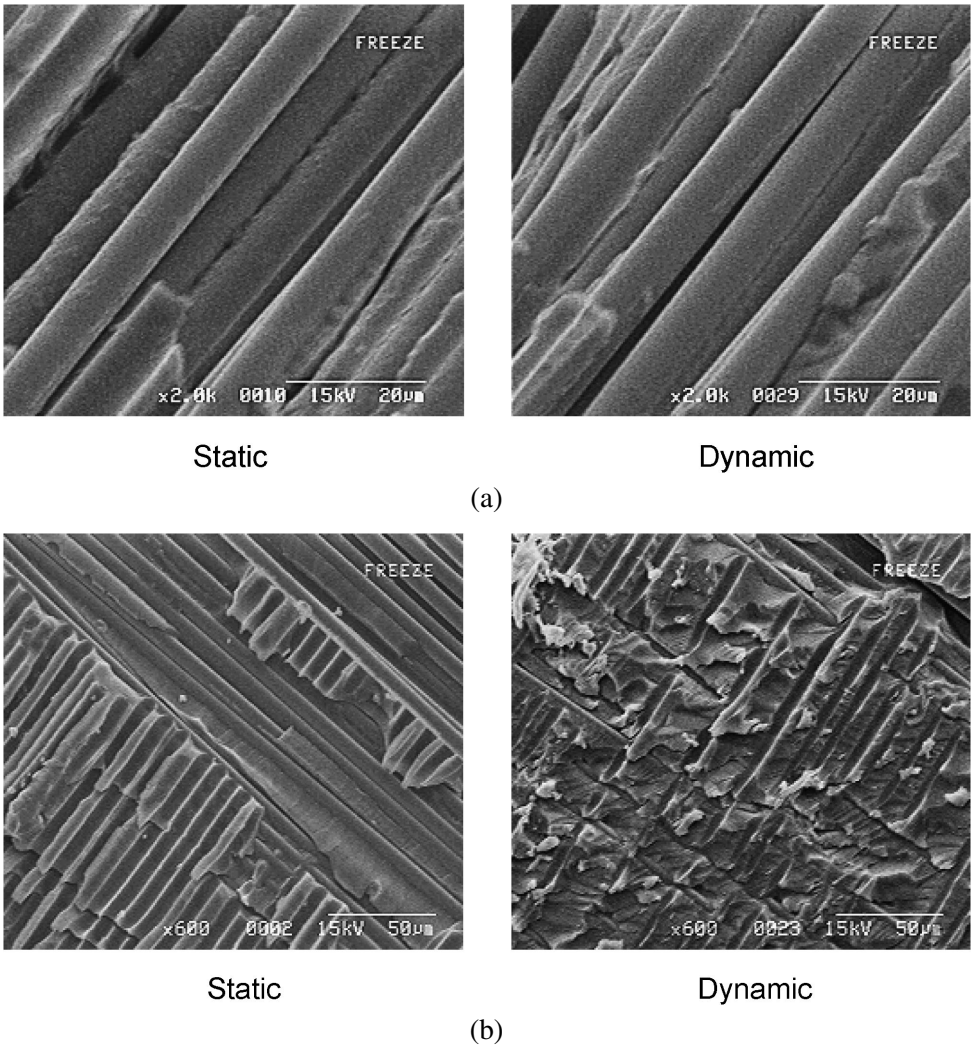

Figure 6. Comparison of the fracture surface behavior between the static and dynamic tests of (a) the 90° specimen; (b) the $[\pm 45]_s$ specimen.

the oblique angle ϕ can be expressed as follows:

$$\cot \phi = -\frac{\bar{S}_{16}}{\bar{S}_{11}}, \tag{3}$$

where $\bar{S}_{ij}$ denotes the compliance coefficients with respect to the xy coordinate system. The oblique angles calculated at the static condition, $\dot{\varepsilon} = 50\ \mathrm{s}^{-1}$, and $\dot{\varepsilon} = 100\ \mathrm{s}^{-1}$ are shown in Fig. 7 as a function of the fiber orientation angle. The elastic moduli and strength for the above strain rates used in this study are also shown in Table 2, where Poisson's ratio is assumed to be constant. The average

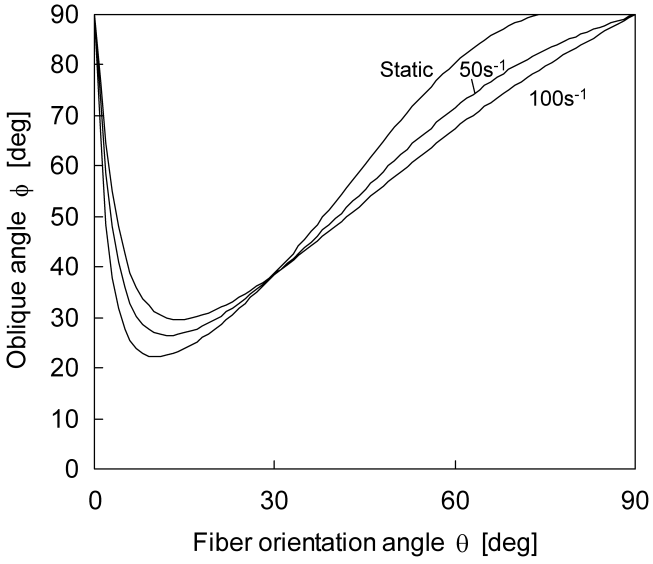

Figure 7. Calculated oblique angle for the static condition, strain rate of 50 s^{-1}, and strain rate of 100 s^{-1}.

Table 2.
Elastic moduli and strength for each strain rate used in this study

	Static condition	Strain rate: 50 s^{-1}	Strain rate: 100 s^{-1}
E_{11} [GPa]	125	125	125
E_{22} [GPa]	9.38	9.88	10.6
G_{12} [GPa]	4.28	6.04	7.59
ν_{12}	0.32	0.32	0.32
X [GPa]	2.36	2.36	2.36
Y [MPa]	63.1	68.1	74.4
S [MPa]	51.3	69.6	91.1

oblique angles for the 15°, 430°, 45°, 60° and 75° off-axis tensile specimens are 26°, 38°, 55°, 73° and 84°, respectively. In order to check the validity of the oblique tab, the strain distribution in the specimens is measured. Figure 8(a) and (b), shows a comparison of the strain of the 15° off-axis specimen in the case of conventional and oblique tabs. The specimen geometry and strain gauge positions are also shown. In Fig. 8(a), it can be seen that the strain-gauge outputs do not coincide with one another. This phenomenon indicates that the strain distribution is not uniform in the case of conventional tabs. It causes a premature failure at the tabbed area due to stress concentration. On the other hand, the strain distribution is almost uniform when oblique tabs are employed. Further, it is found that the failure position is mainly in the gauge section of the specimen. This result is encouraging because it implies that the oblique tab is applicable for evaluating the dynamic tensile strength of off-axis specimens. It is worthwhile to note that the strain distributions for the 60° and 75° off-axis specimens in the case of conventional and oblique tabs are not

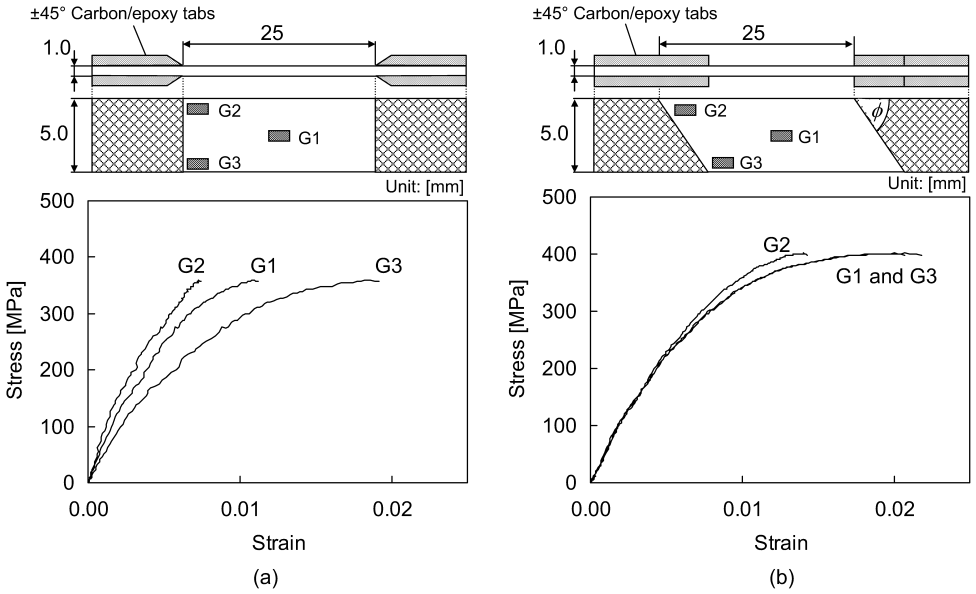

Figure 8. (a) Comparison of the strain for the 15° specimen with conventional tabs (strain rate: 100 s^{-1}). (b) Comparison of the strain for the 15° specimen with oblique tabs (strain rate: 100 s^{-1}).

significantly different from each other; this is because the extension-shear coupling effect is quite small. The failure positions in the case of both the tabs are in the gauge section. Therefore, the conventional tab is also applicable for the 60° and 75° off-axis specimens. Figure 9(a)–(c), present the tensile stress-strain curves for 0°, 15°, 30°, 45°, 60°, 75°, and 90° specimens at the static condition, $\dot{\varepsilon} = 50\ s^{-1}$, and $\dot{\varepsilon} = 100\ s^{-1}$. Table 3 presents a summary of the tensile strength at each strain rate. These results imply that the tensile strength of off-axis specimens increases with the strain rate. The higher fiber orientation specimens produce the more significant contribution to the strain-rate dependence of tensile strength.

4.3. Discussion of the failure criterion

In order to predict the failure criterion under a high-strain-rate condition, the Tsai–Hill failure criterion, which is defined as follows, should be discussed:

$$\frac{\sigma_1^2}{X^2} - \frac{\sigma_1\sigma_2}{X^2} + \frac{\sigma_2^2}{Y^2} + \frac{\tau_{12}^2}{S^2} = 1, \tag{4}$$

where X, Y and S indicate the strength in the longitudinal, transverse, and shear directions, respectively.

Under the unidirectional loading condition, the substitution of the stress transformation equations in equation (4) yields the Tsai–Hill criterion as shown below.

$$\frac{\cos^4\theta}{X^2} + \left(\frac{1}{S^2} - \frac{1}{X^2}\right)\cos^2\theta\sin^2\theta + \frac{\sin^4\theta}{Y^2} = \frac{1}{\sigma_x^2}. \tag{5}$$

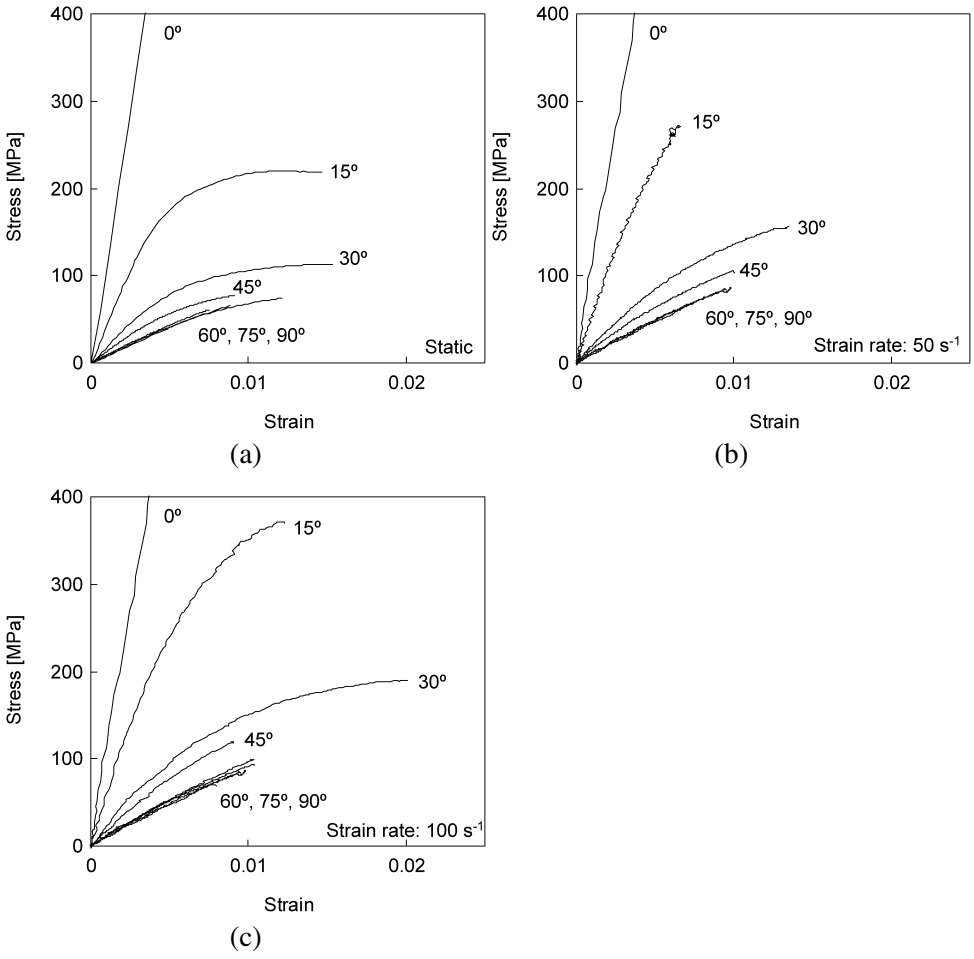

Figure 9. Stress–strain curves for the 0°, 15°, 30°, 45°, 60°, 75° and 90° specimens (a) under the static condition; (b) at a strain rate of 50 s^{-1}; (c) at a strain rate of 100 s^{-1}.

Table 3.
Summary of the tensile strength for each strain rate

Fiber orientation angle	Static condition	Strain rate: 50 s^{-1}	Strain rate: 100 s^{-1}	Increasing ratio at strain rate of 100 s^{-1} (%)
15° [MPa]	218	276	379	73.7
30° [MPa]	113	150	183	61.1
45° [MPa]	80.9	102	121	49.5
60° [MPa]	70.3	86.5	98.1	39.5
75° [MPa]	65.1	81.7	90.9	39.6

The results obtained from this criterion are plotted in Fig. 10 against the experimental data obtained at the static condition, $\dot{\varepsilon} = 50\ s^{-1}$, and $\dot{\varepsilon} = 100\ s^{-1}$. It is concluded that the tensile strength can be characterized quite well using the Tsai–

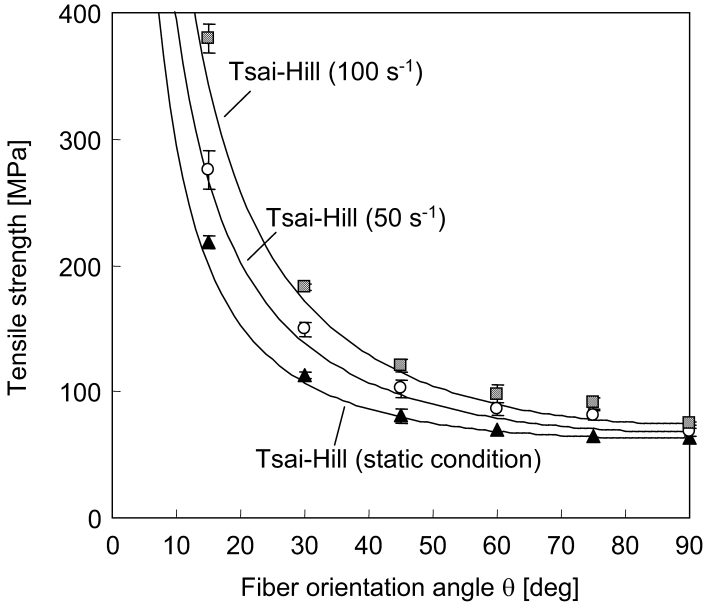

Figure 10. Comparison of the experimental and predicted tensile strength at the static condition, strain rate of 50 s^{-1}, and strain rate of 100 s^{-1} for off-axis specimens.

Hill failure criterion. However, it is important to note that for specimens with lower fiber orientation, the lines predicted at $\dot{\varepsilon} = 50\ s^{-1}$ and $100\ s^{-1}$ cannot adequately represent the experimental data. As shown clearly in Fig. 6, the strain-rate dependence of the transverse tensile strength is mainly affected by the dynamic properties of the fiber/epoxy interface. In contrast, that of the shear strength is mainly affected by not only the interfacial properties but also the dynamic properties of the matrix itself since the fracture surface configuration translates with the strain rate. In other words, the entire tensile strength of a unidirectional CFRP laminate under a high strain rate involves the translation of the fracture mechanism with the strain rate. There is clearly the possibility of a large error between the predicted and experimental values when the strain rate becomes much higher, such as $\dot{\varepsilon} \gg 100$. This result implies that the application limit of the Tsai–Hill failure criterion exists for the prediction of the tensile strength under a high-strain-rate condition.

5. CONCLUSIONS

The following conclusions can be drawn from the present study.

(1) The tensile properties of a unidirectional CFRP laminate under a high strain rate can be evaluated by using the SHB method with a special fixture for the impact tensile specimen.

(2) The tensile modulus and strength in the longitudinal direction are independent of the strain rate. In contrast, the above properties in the transverse direction

and the shear properties increase with the strain rate. Further, the strain-rate dependence of the shear strength is much stronger than that of the transverse strength.

(3) An oblique tab is applicable for measuring the dynamic tensile properties of off-axis specimens.

(4) For off-axis tensile tests under a high strain rate, specimens with higher fiber orientation produce the more significant contribution to the strain-rate dependence of tensile strength.

(5) The Tsai–Hill criterion is applicable for characterizing the tensile strength under a high strain rate. However, the application limit of this criterion also exists for a high-strain-rate condition.

REFERENCES

1. T. Nishiwaki, Designing of CFRP baseball bats, *SAMPE Journal* **38**, 80–82 (2002).
2. N. Taniguchi, T. Nishiwaki and H. Kawada, Evaluating the mechanical properties of a CFRP tube under a lateral impact load using the split Hopkinson bar, *Adv. Compos. Mater.* **14**, 263–276 (2005).
3. G. H. Staab and A. Gilat, High strain rate response of angle-ply glass/epoxy laminates, *J. Compos. Mater.* **29**, 1308–1320 (1995).
4. J. Harding and Y. L. Li, Determination of interlaminar shear strength for glass/epoxy and carbon/epoxy laminates at impact rates of strain, *Compos. Sci. Technol.* **45**, 161–171 (1992).
5. J. Tsai and C. T. Sun, Dynamic compressive strength of polymeric composites, *Int. J. Solids Struct.* **41**, 3211–3224 (2004).
6. B. W. Rosen, Mechanics of composite strengthening, in: *Fiber Composites Materials*. American Society of Metals, Metals Park, OH, pp. 35–75 (1965).
7. J. Harding and L. M. Welsh, A testing technique for fibre-reinforced composites at impact rates of strain, *J. Mater. Sci.* **18**, 1810–1826 (1983).
8. S. V. Thiruppukuzhi and C. T. Sun, Models for the strain-rate-dependent behavior of polymer composites, *Compos. Sci. Technol.* **61**, 1–12 (2001).
9. C. A. Ross, W. H. Cook and L. L. Wilson, Dynamic tensile tests of composite materials using a split-Hopkinson pressure bar, *Exper. Technol.* 30–33 (1984).
10. T. Yokoyama, Impact tensile stress–strain characteristics of wrought magnesium alloys, *Strain* **39**, 167–175 (2003).
11. ASTM D3518
12. K. F. Graff, *Wave Motion in Elastic Solids*. Dover Publications, ISBN 0-486-66745-6 (1991).
13. J. Harding, Effect of strain rate and specimen geometry on the compressive strength of woven glass-reinforced epoxy laminates, *Composites* **24**, 323–332 (1993).
14. C. T. Sun and S. P. Berreth, A new end tab design for off-axis tension test of composite materials, *J. Compos. Mater.* **22**, 766–779 (1988).
15. C. T. Sun and I. Chung, An oblique end-tab design for testing off-axis composite specimens, *Composites* **24**, 619–623 (1993).
16. F. Pierron and A. Vautrin, The 10° off-axis tensile test: a critical approach, *Compos. Sci. Technol.* **56**, 483–488 (1996).
17. F. Pierron, E. Alloba, Y. Surrel and A. Vautrin, Whole-field assessment of the effects of boundary conditions on the strain field in off-axis tensile testing of unidirectional composites, *Compos. Sci. Technol.* **58**, 1939–1947 (1998).